Charge Transfer Hot Paper

International Edition: DOI: 10.1002/anie.201502482
German Edition: DOI: 10.1002/ange.201502482

Carbon Nanodots: Supramolecular Electron Donor–Acceptor Hybrids Featuring Perylenediimides**

*Volker Strauss, Johannes T. Margraf, Konstantin Dirian, Zois Syrgiannis, Maurizio Prato, Cordula Wessendorf, Andreas Hirsch, Timothy Clark, and Dirk M. Guldi**

Abstract: *We describe the formation of charge-transfer complexes that feature electron-donating carbon nanodots (CND) and electron-accepting perylenediimides (PDI). The functionalities of PDIs have been selected to complement those of CNDs in terms of electrostatic and π-stacking interactions based on oppositely charged ionic head groups and extended π-systems, respectively. Importantly, the contributions from electrostatic interactions were confirmed in reference experiments, in which stronger interactions were found for PDIs that feature positively rather than negatively charged head groups. The electronic interactions between the components in the ground and excited state were characterized in complementary absorption and fluorescence titration assays that suggest charge-transfer interactions in both states with binding constants on the order of $8\times10^4\,M^{-1}$ (25 $L\,g^{-1}$). Selective excitation of the two components in ultrafast pump probe experiments gave a 210 ps lived charge-separated state.*

Carbon is the key to many technological applications, from drugs to synthetic materials, that have become indispensable in our daily life and have influenced the world's civilization for centuries.[1] Importantly, the structural diversity of organic compounds and molecules results in endless variations of chemical and physical properties.[2,3] Altering the periodic binding motifs in networks of sp^3-, sp^2-, and sp-hybridized carbon atoms represents the conceptual starting point for constructing a wide palette of carbon allotropes.[4] To this end, the past two decades have served as a test-bed for measuring the physico-chemical properties of carbon in reduced dimensions starting with the advent of fullerenes (0D), followed, in chronological order, by carbon nanotubes (1D), graphene (2D), and recently carbon nanodots (0D/2D).[5,6] These species are now poised for use in a wide range of applications.[1]

The design of new, simple, and inexpensive photosensitizers is important, especially in the conversion of solar energy for emerging areas, such as light harvesting, energy storage, and sensors.[2,8–11] In this context, exploring novel carbon materials based on light-absorbing and/or light-emitting charge-transfer states is expected to play a key role.[12] One versatile strategy en route to charge-transfer states is to combine molecular building blocks that are complementary in terms of electronic levels and binding motifs.[13–16] In this context, carbon nanodots (CND) represent an established class of molecular materials that has recently shown great promise for solar-energy conversion.[17,18] CNDs are strong light emitters that feature broad and, more importantly, tunable absorptions throughout the visible range of the solar spectrum.[19] The basis for a comprehensive understanding of the CNDs' photophysical properties has been laid out in a number of combined experimental and/or theoretical studies.[20]

Both bottom-up and top-down approaches to the synthesis of CNDs have been described in recent years. Thermal or microwave-assisted and electrochemical deposition syntheses are prominent examples for bottom-up approaches, while synthetic strategies, such as the oxidation of graphite and cage opening of fullerenes, typify top-down strategies.[21–23] Whatever the synthesis route, the sizes of CNDs typically range from 1–10 nm with different numbers of stacked graphene layers that are saturated with functional groups at their periphery. Importantly, their facile synthesis and low cost make CNDs promising replacements for expensive organic dyes in optoelectronic applications.[21,24–28]

The charge-transfer activity of CNDs has recently been explored, both in ground and excited states,[27,29] for the excited states this was done in conjunction with a variety of electron donors and acceptors.[26,30] For instance, CNDs have been used together with complementary forms of nanocarbons, such as fullerenes, carbon nanotubes, graphene, in tailored charge-transfer systems. In a leading example, CNDs have been combined with single-walled carbon nanotubes

[*] V. Strauss, J. T. Margraf, K. Dirian, Dr. C. Wessendorf, Prof. Dr. A. Hirsch, Prof. Dr. D. M. Guldi
Department of Chemistry and Pharmacy & Interdisciplinary Center for Molecular Materials (ICMM)
Friedrich-Alexander-Universität Erlangen-Nürnberg
Egerlandstrasse 3, 91058 Erlangen (Germany)
E-mail: dirk.guldi@fau.de
J. T. Margraf, Prof. Dr. T. Clark
Computer-Chemie-Centrum & Interdisciplinary Center for Molecular Materials (ICMM), Friedrich-Alexander-Universität Erlangen-Nürnberg, Nägelsbachstrasse 25, 91058 Erlangen (Germany)
Dr. Z. Syrgiannis, Prof. Dr. M. Prato
Center of Excellence for Nanostructured Materials (CENMAT), Università degli Studi di Trieste
Dipartimento di Scienze Farmaceutiche
Piazzale Europa 1, 34127 Trieste (Italy)

[**] This work was supported by the Deutsche Forschungsgemeinschaft as part of SFB 953 "Synthetic Carbon Allotropes" and of the Excellence Cluster "Engineering of Advanced Materials" and the Bayerische Staatsregierung for funding "Solar Technologies go Hybrid" initiative. J.T.M. is supported by a Beilstein Foundation Scholarship. V.S. is supported by the "Universität Bayern e.V.". This work was also supported by the European Union (Grant FP7-NMP CARINHYPH) and by the Italian Ministry of Education MIUR (FIRB "NanoSolar" RBAP11C58Y, PRIN "Hi-Phuture" 2010N3T9M4_001).

Supporting information for this article is available on the WWW under http://dx.doi.org/10.1002/anie.201502482.

(SWCNTs) affording supramolecular nanohybrids, in which the components function as electron donors and acceptors.[31] Graphene-oxide/CND and methylviologen/CND nanohybrids—brought together by electrostatic interactions—have also been found to feature remarkable charge-transfer activity.[27,30]

We recently reported a novel synthetic approach that gives uniform approximately 1 nm CNDs.[26] Moreover, we demonstrated that CNDs form stable charge-transfer hybrids with either electron donors or acceptors. The mutual electron donor–acceptor interactions can be fine-tuned using electrostatic interactions with the negatively charged edge groups of CNDs. Furthermore, the central units of the CND layers feature extended π-systems, which is susceptible for π-stacking interactions.

Perylenediimides (PDI) can complement CNDs to form charge-transfer complexes because they are strong electron acceptors and also feature an extended π-system.[32,33] One great advantage of PDIs is their broad range of possible functionalization, which allows their structural and electronic properties to be tailored.[34,35] For instance, PDIs are easily functionalized with positively or negatively charged head groups at the imido-positions.[36–38] We show below that functionalization with positively charged ammonium head groups is critical for stable interactions with negatively charged CNDs. Interactions between CNDs and PDIs in the ground state have been investigated using voltammetry and steady-state absorption spectroscopy. In addition, excited-state dynamics and reactions have been investigated using both steady-state and time-resolved emission spectroscopy and ultrafast pump-probe experiments. Density-functional theory (DFT) and configuration-interaction calculations based on semi-empirical molecular-orbital theory have been used to help clarify the experimental results.

PDIs **1** and **2** were synthesized using a published procedure.[36–38] PDIs **1** and **2** have identical PDI cores, but positive and negatively charged head groups, respectively, at their imido-positions (see Figure 1). PDI **1** is substituted with two positively charged trimethylammonium groups, while **2** bears first-generation, negatively charged Newkome-type dendrons. The following discussion will focus on the experimental results found for **1**, the reference experiments with **2** are described in the Supporting Information.

Figure S1 in the Supporting Information shows the absorption spectrum of **1**, which resembles the typical PDI absorption pattern with maxima at 500 and 533 nm and a shoulder at 470 nm with extinction coefficients as high as $3.0\times10^4\,M^{-1}cm^{-1}$.[39] The inverse intensity distribution amid their vibronic states seen for **1** with the 500 nm peak being stronger than the one at 533 nm, has been assigned to intermolecular collisions.[41] Two well-defined maxima at 545 and 587 nm with an intensity ratio of 2.5:1 are found in the fluorescence spectrum of **1**. The fluorescence quantum yields were determined to be 5.9%, from which we conclude that the fluorescence originates from monomeric rather than aggregated PDIs, in line with the fluorescence lifetime measurements, in which only a single lifetime of 4.7 ns was found.

The absorption and fluorescence spectra of **2** (shown in Figure S2) show similar, but slightly red-shifted characteristics. For example, the absorption maxima occur at 500 and 540 nm and the intensity of the long wavelength maximum is notably weaker than for **1**. The maxima in the fluorescence spectra appear at 548 and 589 nm with an intensity ratio that, again, indicates that monomeric PDIs are the origin of the fluorescence. The extinction coefficient and fluorescence quantum yield, $2.7\times10^4\,M^{-1}cm^{-1}$ and 5.5%, respectively, of **2** are close to those found for **1**.

The pressure-synthesized carbon nanodots (pCNDs) were produced under mild reaction conditions in a microwave reactor (see Experimental Section).[26,40] The absorption spectrum, which is shown in Figure S3, shows a prominent maximum at 339 nm, a shoulder at around 410 nm, and a weak absorption tail reaching into the visible part of the spectrum. The fluorescence spectrum found upon excitation at 350 nm is best described as a broad peak with its maximum at 443 nm. Notably, the pCND fluorescence is biphasic; photoexcitation at 500 nm results in weak features with a maximum at 592 nm, as shown in Figure S3.

The electrochemical characterization was performed using cyclic voltammetry and differential pulse voltammetry. The voltammograms of **1** and pCND, measured against an Ag/AgCl reference electrode, are shown in Figure S4. Neither cyclic nor differential pulse voltammograms of pCND reveal appreciable signals in the reductive voltage region up to −0.8 V in aqueous solution. In stark contrast, **1** shows two reduction waves at 0.5 V and 0.72 V, which we assign to the first and second reductions of **1**, respectively. The re-oxidations occur at −0.34 and −0.27 V in the reverse scan direction. The voltammograms of **2** are shown in Figure S5. No distinct reductions of **2** were discernible in aqueous solution. The first reduction of **2** was detected in methanol at −0.35 V vs. Ag/AgCl.

Steady-state absorption titration assays provided information about the non-covalent assembly of pCND with **1**. The concentration of **1** was kept constant, pCND was added slowly and the absorption changes monitored (Figure 2). A significant decrease of the PDI-centered absorptions between 450 and 600 nm down to 67% of the original intensity is observed with increasing concentrations of pCND. This is a typical indicator for the non-covalent complexation of pCND and **1** to afford pCND/**1**.[42] Moreover, a shift of the absorption maxima from 500 and 535 nm to 502 and 539 nm, respectively, together with the appearance of two isosbestic points at 480 and 557 nm suggests significant electronic communication between pCND and **1**.[43] In contrast, the

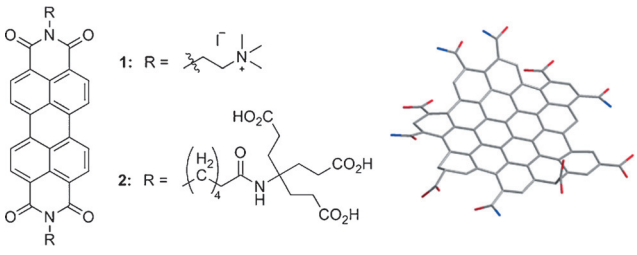

Figure 1. Left: structural formula of PDI **1** and **2**. Right: representative structure of pCND.

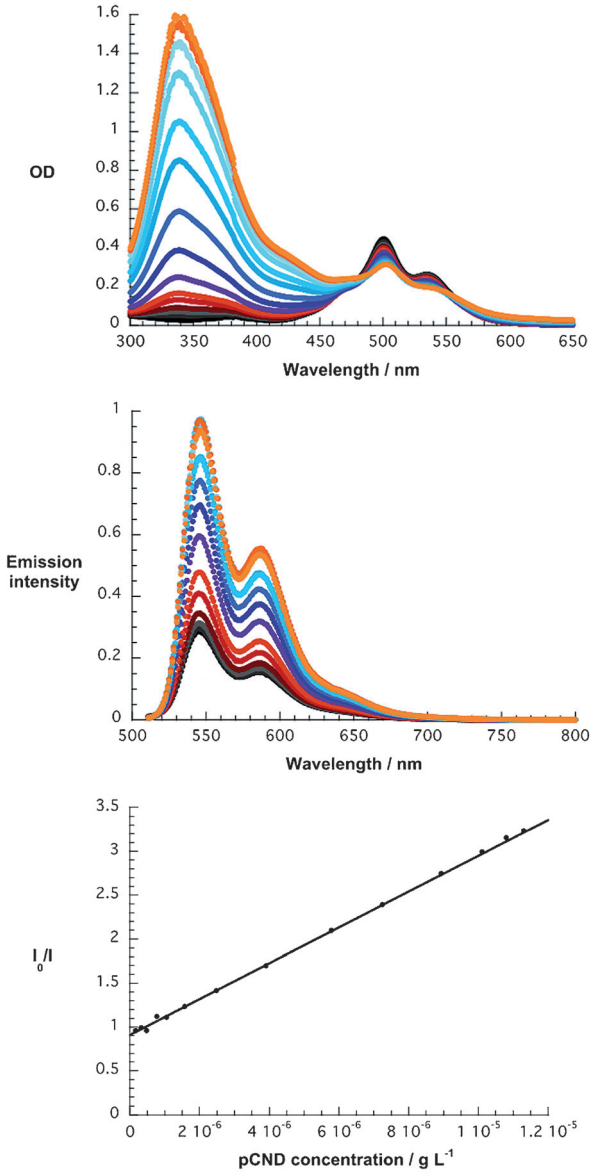

Figure 2. Top: Absorption spectra of **1** (orange, 10^{-5} M) during the course of a titration with pCND (blue > red > black, 0–0.1 g L^{-1}) in phosphate-buffered D_2O (pH 7.2) at room temperature. Middle: fluorescence spectra of **1** (black, 10^{-5} M) during the course of a titration with pCND (red > blue > orange, 0–0.1 g L^{-1}) in phosphate-buffered D_2O (pH 7.2) at room temperature. Bottom: relationship of I_0/I versus the concentration of pCND used to determine the association constant.

lack of changes for PDI-centered absorptions in the corresponding titrations of **2** with pCND up to a concentration of 0.1 g L^{-1} indicates neither complexation nor ground-state interactions, as shown in Figure S7 of the Supporting Information.

PDI **1** can be excited selectively at 500 nm. Addition of pCND to **1** leads to an exponential quenching of the PDI-centered fluorescence as shown in the Stern–Volmer plot (Figure 2), which indicates a binding constant of 25 L g^{-1}. Finally, the fluorescence decay in the resulting pCND/**1** is best fit by a two-exponential decay function with lifetimes of 0.3 and 4.7 ns with a relative weight distribution of 0.15 to 0.85. In analogous titration experiments with **2** and variable pCND concentrations, only a very weak fluorescence quenching is discernable (Figure S8).

To analyze the photophysical changes of pCND further, reversed titrations using a constant concentration of pCND and variable amounts of **1** were conducted. The most striking observation in the absorption titration assays is the strong decrease in pCND-centered absorptions (Figure S9). Again, a change in absorption is a reliable indicator of electronic interactions between pCND and **1**. A careful analysis of the pCND absorption features reveals a concentration-dependent blue shift from 339 to 337 nm and formation of a 375 nm shoulder. In line with the evidence discussed above, pCND and **2** show no evidence of interactions (Figure S10).

Steady-state fluorescence assays indicate that the addition of **1** causes strong quenching of the pCND fluorescence. Note that 350 nm radiation excites both components, so that pCND and **1** both fluoresce, which was taken into account during the quantitative analyses. Figure S11 shows the Stern–Volmer plot obtained, which deviates to higher values than expected for a linear dependence at higher concentrations of **1**. This deviation suggests that, in addition to static quenching in pCND/**1** with a binding constant of 8.0×10^4 M^{-1}, collisional quenching between pCND and **1** is operative. As in the absorption assays, a considerable blue shift of the fluorescence from 443 to 439 nm and a narrowing is found (Figure S12). Once again, spectral changes found in the titration assays between pCND and **2**, are barely detectable, (Figure S12).

The role of the ionic interactions as a binding motif between **1** and pCND was investigated by steadily increasing the ionic strength of the solution by adding potassium chloride. In non-buffer solution, a fluorescence quenching to 15% relative to pure **1** was found for pCND/**1**. Upon addition of KCl, the fluorescence recovered partially to a value of 23% (Figure S13). A blue-shift of the maxima (Figure S14) is found in the absorption spectra of the complex. However, neither the extinction nor the fluorescence of **1** recovered fully.

To obtain further information about ground-state interactions between pCND and **1**, we recorded voltammograms of different mixtures of pCND and **1**. Note that oxidation signals of pCND can be only detected in polar organic solvents, such as MeOH or DMSO, and appear in the positive voltage region between 0.6 and 1.2 V. Because of this, we focused on the cathodic scans, in which only the one-electron reduction of **1** takes place. Figure S15 shows a significant shift of the one-electron reduction of **1** towards more negative potentials upon addition of pCND. This implies a shift of electron density from the electron-donating pCNDs to **1** that renders the reduction of the **1** more difficult. Plots of the shift in the reduction potential versus the pCND concentration show a clear exponential dependence that corresponds to a binding constant of approximately 50 L g^{-1}.

Density-functional theory (DFT) calculations at the PBE + D/DNP level with the Tkatchenko and Scheffler dispersion correction[44–46] were used to help elucidate the nature of the interaction between **1** and pCNDs. Water

solvation was considered implicitly using the COSMO model.[47] All calculations were performed with dMol3.[46,48] As in our previous work on pCNDs, we based the models on heavily functionalized graphene fragments.[26] In this case, we added two carboxylate groups to form neutral complexes with **1**. We used three pCND models that differed only in the location of the carboxylate groups leading to different complexes with **1** as shown in Figure 3.

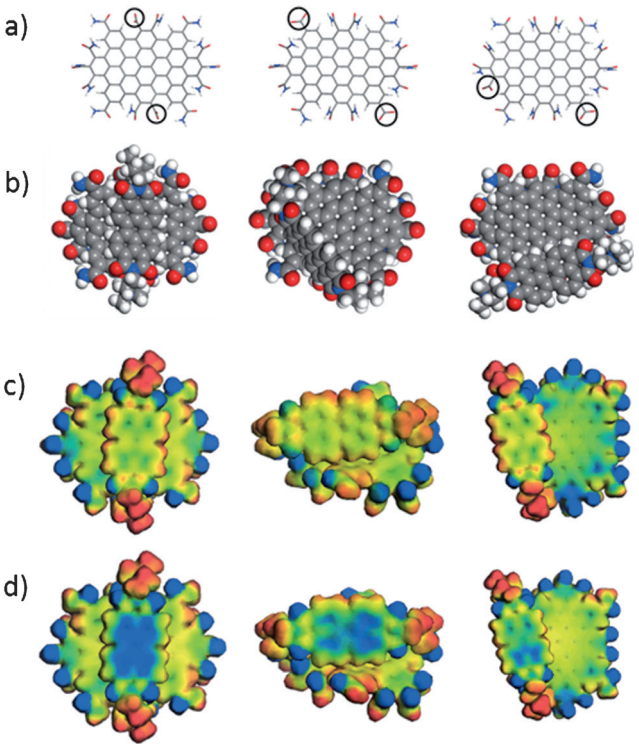

Figure 3. a) Structures of the pCND models, the carboxylate groups are marked with black circles. b) pCND/**1** complexes referred to as top (left), diagonal (center), and side (right), according to the orientation of **1** relative to pCND. c) Ground-state molecular electrostatic potentials of pCND/**1** complexes. d) Molecular electrostatic potentials of the respective lowest energy charge-transfer states. Color code from −0.2 (blue) to 0.2 (red) Hartree e^{-1}.

The complexes are formed either mainly through ionic interactions between the ammonium and carboxylate groups (diagonal and side geometry) or through mixed ionic/π–π interactions (in the top geometry). The top geometry is energetically favored, with an interaction energy of −51.3 kcal mol^{-1} compared to −30.5 and −26.6 kcal mol^{-1} for the diagonal and side geometries, respectively. However, our pCND model is somewhat idealized; the formation of mixed ionic/π–π complexes may be hindered by greater steric repulsion in the real case.

We then performed semi-empirical configuration interaction with single excitations (CIS) calculations on these systems to understand the effect of the complex orientation on the nature of the pCND/**1** charge-transfer state. These calculations were performed with VAMP using the PM6 Hamiltonian.[49,50] The calculations reproduced the experimental UV/Vis spectrum of **1** quite well (Figure S16). The lowest energy charge-transfer state shows charge shift from the pCND to **1** in all cases (Figure 3). The excitation energies show a similar dependence on the complex geometry to the interaction energies. The calculated vertical excitation energies are 2.9 eV for the top orientation, 4.0 and 3.8 eV for the diagonal and side orientations, respectively.

Thus photoinduced charge separation is a likely cause for the emission quenching observed in pCND/PDI complexes, independent of the binding motive. The spatial contact between the π-systems in the top geometry stabilizes the charge-separated state.

Fluorescence lifetime measurements using time-correlated single-photon counting (TCSPC) showed the addition of pCND to exert considerable impact on the excited-state lifetimes of **1** (Figure S17). In the absence of pCND, the singlet excited state decays mono-exponentially with a lifetime of 4.7 ns. In the presence of pCND, two lifetimes of 4.7 and 0.2 ns were found. Note that the mass ratio of pCND to **1** was less than 1:5 to avoid full quenching of the fluorescence of **1**. We assign the long lifetime of 4.7 ns to free, uncomplexed **1** and the 0.2 ns lifetime to a deactivation in pCND/**1** through electron transfer. Complementary lifetime measurements showed that the lifetimes of **2** remained unchanged upon addition of pCND in a concentration of up to 0.05 g L^{-1} (Figure S18).

Femtosecond transient-absorption measurements following excitation at either 387 or at 500 nm allowed selective excitation of pCND or **1**/**2**, respectively. For **1**, 500 nm excitation leads to the instantaneous formation of a strong minimum at 498 nm and several maxima at 543, 590, 735, and 963 nm (Figure S19). The minimum represents the ground-state bleaching as it is the inverse of the absorption spectrum. We assign the positive transients ranging from 543 to 1200 nm to excited-state absorptions. Multi-wavelength lifetime analyses yield two dominant components of 150 and 300 ps. Figure S20 shows that the pump-probe experiments with **2** exhibited similar deactivation behavior. Lifetimes of 20 and 330 ps underline, once again, the resemblance to the electronic structure of **1**.

Typical features of reduced **1** at 703, 825, and 990 nm are found in femtosecond transient absorption measurements with pCND/**1** (Figure 4). Moreover, the ground-state bleaching at 500 nm is significantly weaker. Furthermore, the presence of pCND strongly influences the lifetime of the transient absorptions. A global fitting of the transient absorptions yielded a short lifetime of 4 ps and a longer one of 210 ps. The long-lived component does not change at different concentrations of pCND. Therefore, it is safe to assign the long component to anion-related features. Consistent with the observations from the steady-state spectrophotometric and voltammetric titrations, the immediate formation of the anion-related signatures points to instantaneous complex formation. Analogous behavior was seen upon excitation at 387 nm (Figures S22, S23). However, strong superimpositions with the excited-state absorptions of pCND dominate the spectra. No anion-related signals were detected in the reference experiments with **2** and pCND (Figure S21, S25); the excited-state absorption pattern of **2** remains unchanged upon addition of different amounts of

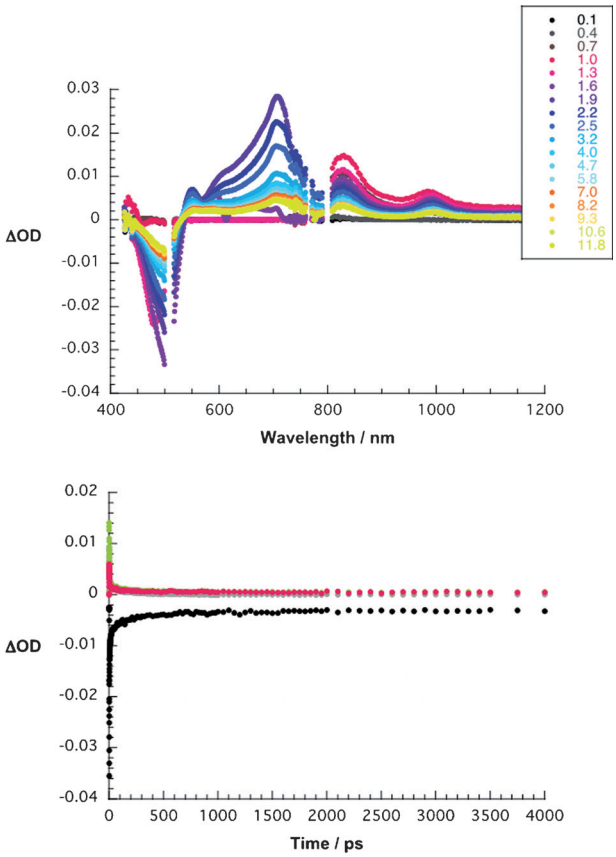

Figure 4. Top: differential absorption spectra obtained upon femtosecond pump probe experiments (500 nm) of pCND/**1** (1×10^{-5} M) in phosphate-buffered D_2O (pH 7.2) with several time delays in ps between 0 and 12 ps (gray > red > blue > orange > yellow) at room temperature. Bottom: time absorption profiles of the spectra shown in the above at 500 nm (black), 591 nm (gray), 850 nm (green), and 1000 nm (magenta) monitoring the charge separation and charge recombination.

pCND. Moreover, a multi-wavelength lifetime analysis confirms that the presence of pCNDs does not affect the excited-state deactivation of **2**.

The versatility of newly pressure-synthesized carbon nanodots (pCND) featuring electron-donation ability and negatively charged edge groups was explored in self-assembling electron donor–acceptor hybrids. pCNDs were combined with electron-accepting and positively charged perylenediimides (PDI) **1**, by virtue of ionic and π–π interactions to afford pCND/**1**. The binding constants are as high as $8\times10^4\,M^{-1}$ and/or $25\,L\,g^{-1}$. For pCND/**1**, corroboration of ionic interactions between the carboxylate and ammonium groups, and for π–π interactions, came from DFT calculations. In reference experiments, in which negatively charged PDI **2** were tested, pCNDs gave no notable spectral changes. Moreover, we infer sizeable charge shift from the pCNDs to **1** in the ground state from configuration–interaction calculations. In the excited state of pCND/**1**, which was probed by steady-state/time-resolved fluorescence spectroscopy and femtosecond transient-absorption spectroscopy, PDI fluorescence quenching results in charge separation to afford the one-electron oxidized pCND and the one-electron reduced **1**. The charge separated state lifetime in pCND/**1** is 210 ps and as such comparable to those found in SWCNT/PDI nanohybrids with values ranging from 170 to 300 ps.[32,42]

Keywords: carbon nanodots · charge transfer · donor–acceptor compounds · perylenediimides · transient absorption

How to cite: *Angew. Chem. Int. Ed.* **2015**, *54*, 8292–8297
Angew. Chem. **2015**, *127*, 8410–8415

[1] D. Jariwala, V. K. Sangwan, L. J. Lauhon, T. J. Marks, M. C. Hersam, *Chem. Soc. Rev.* **2013**, *42*, 2824.
[2] T. Torres, G. Bottari, *Organic Nanomaterials*, Wiley, Hoboken, **2013**.
[3] V. Balzani, A. Credi, M. Venturi, *Molecular Devices and Machines: Concepts and Perspectives for the Nanoworld*, Wiley-VCH, Weinheim, **2008**.
[4] E. H. L. Falcao, F. Wudl, *J. Chem. Technol. Biotechnol.* **2007**, *82*, 524.
[5] H. Li, X. He, Z. Kang, H. Huang, Y. Liu, J. Liu, S. Lian, C. H. A. Tsang, X. Yang, S.-T. Lee, *Angew. Chem. Int. Ed.* **2010**, *49*, 4430; *Angew. Chem.* **2010**, *122*, 4532.
[6] P. Miao, K. Han, Y. Tang, B. Wang, T. Lin, W. Cheng, *Nanoscale* **2015**, *7*, 1586.
[7] T. Akasaka, W. Fred, S. Nagasu, *Chemistry of Nanocarbons*, Wiley, Hoboken, **2010**.
[8] M. Pumera, *Energy Environ. Sci.* **2011**, *4*, 668.
[9] C. Gao, Z. Guo, J.-H. Liu, X.-J. Huang, *Nanoscale* **2012**, *4*, 1948.
[10] W. Putzbach, N. J. Ronkainen, *Sensors* **2013**, *13*, 4811.
[11] K. Dirian, M. Á. Herranz, G. Katsukis, J. Malig, L. Rodríguez-Pérez, C. Romero-Nieto, V. Strauss, N. Martín, D. M. Guldi, *Chem. Sci.* **2013**, *4*, 4335.
[12] a) D. M. Guldi, R. D. Costa, *J. Phys. Chem. Lett.* **2013**, *4*, 1489; b) S. Kirner, M. Sekita, D. M. Guldi, *Adv. Mater.* **2014**, *26*, 1482.
[13] H. Isla, B. Grimm, E. M. Pérez, M. Rosario Torres, M. Ángeles Herranz, R. Viruela, J. Aragó, E. Ortí, D. M. Guldi, N. Martín, *Chem. Sci.* **2012**, *3*, 498.
[14] B. Grimm, J. Schornbaum, H. Jasch, O. Trukhina, F. Wessendorf, A. Hirsch, T. Torres, D. M. Guldi, *Proc. Natl. Acad. Sci. USA* **2012**, *109*, 15565.
[15] K. A. Nielsen, L. Martín-Gomis, G. H. Sarova, L. Sanguinet, D. E. Gross, F. Fernández-Lázaro, P. C. Stein, E. Levillain, J. L. Sessler, D. M. Guldi, et al., *Tetrahedron* **2008**, *64*, 8449.
[16] K. Nielsen, W.-S. Cho, G. H. Sarova, B. M. Petersen, A. D. Bond, J. Becher, F. Jensen, D. M. Guldi, J. L. Sessler, J. O. Jeppesen, *Angew. Chem. Int. Ed.* **2006**, *45*, 6848; *Angew. Chem.* **2006**, *118*, 7002.
[17] H.-J. Ahn, M.-J. Kim, K. Kim, M.-J. Kwak, J.-H. Jang, *Small* **2014**, *10*, 2325.
[18] G.-H. Kim, B. Walker, H.-B. Kim, J. Y. Kim, E. H. Sargent, J. Park, *Adv. Mater.* **2014**, *26*, 3321.
[19] S. Do, W. Kwon, S.-W. Rhee, *J. Mater. Chem. C* **2014**, *2*, 4221.
[20] J. T. Margraf, V. Strauss, D. M. Guldi, T. Clark, *J. Phys. Chem. B* **2015**, DOI: 10.1021/jp510620j.
[21] L. Tang, R. Ji, X. Cao, J. Lin, H. Jiang, X. Li, K. S. Teng, C. M. Luk, S. Zeng, J. Hao, et al., *ACS Nano* **2012**, *6*, 5102.
[22] H. Ming, Z. Ma, Y. Liu, K. Pan, H. Yu, F. Wang, Z. Kang, *Dalton Trans.* **2012**, *41*, 9526.
[23] J. Lu, P. S. E. Yeo, C. K. Gan, P. Wu, K. P. Loh, *Nat. Nanotechnol.* **2011**, *6*, 247.
[24] H. Li, Z. Kang, Y. Liu, S.-T. Lee, *J. Mater. Chem.* **2012**, *22*, 24230.
[25] S. Ghosh, A. I. A. M. Chizhik, N. Karedla, M. O. Dekaliuk, I. Gregor, H. Schuhmann, M. Seibt, K. Bodensiek, I. A. T. Schaap, O. Schulz, et al., *Nano Lett.* **2014**, *14*, 5656.

[26] V. Strauss, J. T. Margraf, C. Dolle, B. Butz, T. J. Nacken, J. Walter, W. Bauer, W. Peukert, E. Spiecker, T. Clark, et al., *J. Am. Chem. Soc.* **2014**, *136*, 17308.
[27] P. Yu, X. Wen, Y.-R. Toh, Y.-C. Lee, K.-Y. Huang, S. Huang, S. Shrestha, G. Conibeer, J. Tang, *J. Mater. Chem. C* **2014**, *2*, 2894.
[28] W. Kwon, G. Lee, S. Do, T. Joo, S.-W. W. Rhee, *Small* **2014**, *10*, 506.
[29] X. Xu, R. Ray, Y. Gu, H. J. Ploehn, L. Gearheart, K. Raker, W. A. Scrivens, *J. Am. Chem. Soc.* **2004**, *126*, 12736.
[30] Y. Song, S. Zhu, S. Xiang, X. Zhao, J. Zhang, H. Zhang, Y. Fu, B. Yang, *Nanoscale* **2014**, *6*, 4676.
[31] V. Strauss, J. T. Margraf, T. Clark, D. M. Guldi, unpublished results.
[32] C. Oelsner, C. Schmidt, F. Hauke, M. Prato, A. Hirsch, D. M. Guldi, *J. Am. Chem. Soc.* **2011**, *133*, 4580.
[33] M. A. Iron, R. Cohen, B. Rybtchinski, *J. Phys. Chem. A* **2011**, *115*, 2047.
[34] Y. Nagao, *Prog. Org. Coat.* **1997**, *2*, 43.
[35] L. Chen, C. Li, K. Müllen, *J. Mater. Chem. C* **2014**, *2*, 1938.
[36] C. D. Schmidt, C. Böttcher, A. Hirsch, *Eur. J. Org. Chem.* **2007**, 5497.
[37] B. Wang, C. Yu, *Angew. Chem. Int. Ed.* **2010**, *49*, 1485; *Angew. Chem.* **2010**, *122*, 1527.
[38] Y. Huang, Y. Yan, B. M. Smarsly, Z. Wei, C. F. J. Faul, *J. Mater. Chem.* **2009**, *19*, 2356.
[39] F. Würthner, Z. Chen, V. Dehm, V. Stepanenko, *Chem. Commun.* **2006**, 1188.
[40] S. Qu, X. Wang, Q. Lu, X. Liu, L. Wang, *Angew. Chem. Int. Ed.* **2012**, *51*, 12215; *Angew. Chem.* **2012**, *124*, 12381.
[41] A. D. Q. Li, W. Wang, L.-Q. Wang, *Chem. Eur. J.* **2003**, *9*, 4594.
[42] C. Ehli, C. Oelsner, D. M. Guldi, A. Mateo-Alonso, M. Prato, C. Schmidt, C. Backes, F. Hauke, A. Hirsch, *Nat. Chem.* **2009**, *1*, 243.
[43] M. Supur, S. Fukuzumi, *J. Phys. Chem. C* **2012**, *116*, 23274.
[44] A. Tkatchenko, M. Scheffler, *Phys. Rev. Lett.* **2009**, *102*, 073005.
[45] J. P. Perdew, K. Burke, M. Ernzerhof, *Phys. Rev. Lett.* **1996**, *77*, 3865.
[46] B. Delley, *J. Chem. Phys.* **1990**, *92*, 508.
[47] A. Klamt, G. Schüürmann, *J. Chem. Soc. Perkin Trans. 2* **1993**, 799.
[48] B. Delley, *J. Chem. Phys.* **2000**, *113*, 7756.
[49] J. J. P. Stewart, *J. Mol. Model.* **2007**, *13*, 1173.
[50] T. Clark, A. Alex, B. Beck, F. Burkhardt, J. Chandrasekhar, P. Gedeck, A. Horn, M. Hutter, B. Martin, P. O. Dral, G. Rauhut, W. Sauer, T. Schindler, T. Steinke, *VAMP 11.0*, *Erlangen* **2011**.

Received: March 17, 2015
Published online: May 27, 2015

